# Theory and Experiment of High-Gain Modified Angular Log-Periodic Folded Waveguide Slow Wave Structure

Duo Xu, *Graduate Student Member, IEEE*, Shaomeng Wang, *Member, IEEE*, Zhanliang Wang, *Member, IEEE*, Wei Shao, Tenglong He, Hexin Wang, Tao Tang, Huarong Gong, *Member, IEEE*, Zhigang Lu, Zhaoyun Duan, *Senior Member, IEEE*, Jinjun Feng, *Senior Member, IEEE*, and Yubin Gong, *Member, IEEE*

***Abstract*— A novel modified angular log-periodic folded waveguide slow wave structure (MALPFW-SWS) is proposed for high-gain traveling wave tubes (TWTs). Each unit of the MALPFW-SWS has different dispersion characteristics and thus it has the ability to suppress oscillations in TWTs. The dispersion equation of the MALPFW-SWS is derived and a Ka-band MALPFW-SWS is designed according to the dispersion equation for verification. The particle-in-cell (PIC) simulation indicated that the output signal is steady even the gain of the designed MALPFW-TWT reaches 40 dB. The frequency spectrum of the output signal also proved that the MALPFW-SWS can suppress oscillations. The cold test experiment results show that the transmission characteristics of the fabricated MALPFW-SWS are good and are in good agreement with the simulation results.**

***Index Terms*— Oscillations suppression, folded waveguide, slow wave structure, traveling wave tube.**

## I. Introduction

FOLDED waveguide [1], a popular SWS with advantages of high-power-capacity and easy machining, has wide applications in high-power TWTs. Many reports on the theory, design, and experiment [2]–[7] of the FW-SWS have been published in recent years.

In theory, the maximal gain of a one-section SWS should be kept lower than 26 dB [8] to avoid the oscillation issues. Therefore, all the SWSs in the designs in [3]–[7] were divided into two sections by the attenuator to suppress oscillations [9], [10]. However, the introducing of the attenuator will bring more difficulties in the fabrication of the TWT, especially for the terahertz TWT due to the small size.

In this letter we proposed a novel MALPFW-SWS as a solution to this problem. The MALPFW-SWS has the ability to suppress oscillations in TWT and can support an ultra-high gain without the attenuator.

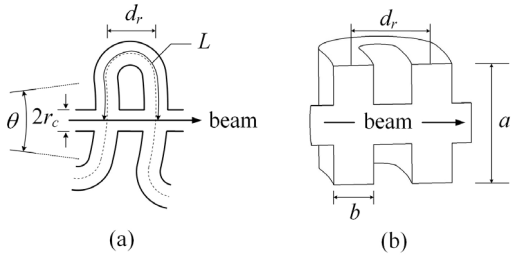


Fig. 1. Sketch of the novel MALPFW-SWS. (a) 2D view of one unit on $r$-$\varphi$ plane; (b) 3D model of one unit.

## II. Theoretical Analysis of the Dispersion Characteristics

The angular log-periodic meander line [11] is a conventional meander path SWS evolved from logarithm helix and has been widely used in planar miniaturized TWT. The proposed MALP meander line can be obtained by using the same evolution progress to process a modified logarithm helix whose path can be described by the equation

$$r = a_0 e^{b_0 \varphi} - r_0 \tag{1}$$

where $r$ and $\phi$ are the coordinates in radial and angular axis, respectively. $r_0$ is the additional value in radial axis.

Fig. 1 shows the sketches of the MALPFW-SWS. The dash line in Fig. 1 (a) represents the meander path of the MLPFW-SWS, the MALP meander line. $d_r$ and $L$ are the beam and wave pathlengths in a unit, respectively. $\theta$ is the angle of the MALP meander line. $a$ and $b$ are the transverse dimensions of the waveguide. $r_c$ is the radius of the cylindrical electron beam tunnel.

According to the path equation (1), the electron beam and electromagnetic wave path lengths in the $n$th unit, $d_{rn}$ and $L_n$,

Manuscript received May 7, 2020; revised June 2, 2020; accepted June 4, 2020. Date of publication June 8, 2020; date of current version July 24, 2020. This work was supported in part by the National Natural Science Foundation of China under Grant 61531010 and Grant 61921002 and in part by the Science and Technology on High Power Microwave Laboratory Fund under Grant 6142605180201. The review of this letter was arranged by Editor H. Mimura. *(Corresponding authors: Shaomeng Wang; Yubin Gong.)*

Duo Xu, Shaomeng Wang, Zhanliang Wang, Wei Shao, Tenglong He, Hexin Wang, Tao Tang, Huarong Gong, Zhigang Lu, Zhaoyun Duan, and Yubin Gong are with the National Key Laboratory of Science and Technology on Vacuum Electronics, University of Electronic Science and Technology of China, Chengdu 610054, China (e-mail: wangsm@uestc.edu.cn; ybgong@uestc.edu.cn).

Jinjun Feng is with the National Key Laboratory of Science and Technology on Vacuum Electronics, Beijing Vacuum Electronics Research Institute, Beijing 100015, China.

Color versions of one or more of the figures in this letter are available online at http://ieeexplore.ieee.org.

Digital Object Identifier 10.1109/LED.2020.3000759

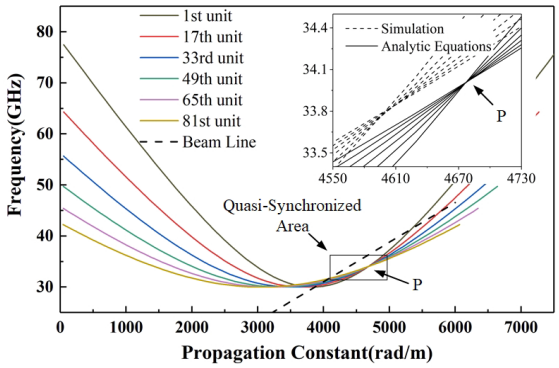


Fig. 2. Dispersion curves of the fundamental mode of the MALPFW-SWS units.

can be written as

$$d_{rn} = a_0(e^{2b_0\pi} - 1)e^{2b_0(n-1)\pi} = d_{r1}e^{2b_0(n-1)\pi} \quad (2)$$

$$L_n = \frac{a_0}{b_0}\left(e^{\frac{b_0\theta}{2}} - 1\right)\left(1 + e^{2b_0\pi}\right)e^{2b_0(n-1)\pi} + \frac{d_{rn}\pi}{2} - r_0\theta = (L_1 + r_0\theta)e^{2b_0(n-1)\pi} - r_0\theta \quad (3)$$

A simplified dispersion equation of the $TE_{10}$ mode was derived in [2] by a smooth-wall FW-SWS model, which is:

$$\omega = c\sqrt{\left(\frac{\beta_{zm}d_r - \pi - 2m\pi}{L}\right)^2 + \left(\frac{\pi}{a}\right)^2} \quad (4)$$

where, $\omega$ is the angular frequency of the wave, $\beta_{zm}$ is the longitudinal propagation constant (rad/m) of the $m$th spatial harmonic and $c$ is the speed of light in vacuum.

Substituting $d_r$ and $L$ into (4), we can find a common intersection point P for these dispersion curves, as shown in Fig. 2. We therefore name it as the Perfect-Synchronized Point (PSP) with the coordinates

$$\left(\frac{\pi(L_1 + r_0\theta)}{r_0\theta d_{r1}}, c\sqrt{\left(\frac{\pi}{r_0\theta}\right)^2 + \left(\frac{\pi}{a}\right)^2}\right) \quad (5)$$

related to the dimensions of $r_0$, $d_{r1}$, $L_1$ and $\theta$. The corresponding frequency is called Perfect-Synchronized frequency (PSF).

For electromagnetic wave with a specified frequency different from the PSF, the phase velocity varies with $n$, partly like the feature of conventional phase velocity tapered SWSs. When the specified frequency is lower than the PSF, the phase velocity is positively tapered and it turns to be negatively tapered once the frequency is higher than the PSF, as shown in Fig. 3(a). Fig. 3(b) gives the relationship between the phase velocity and axial position at 31.38 GHz, 34.01 GHz and 35.44 GHz, respectively.

Quasi-Synchronized Area (QSA) is the effective interaction area of the MALPFW-SWS. The frequency range of QSA is defined by two different ways for its two ends.

For the lower frequency end, the phase velocity is positively tapered. An average spread of the positive tapering is about 8% [12]–[15], and it was adopted as the spread limitation of the lower frequency end in this letter.

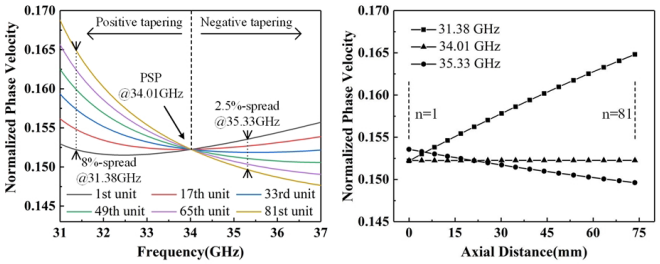


Fig. 3. The variations of phase velocity with (a) frequency and (b) axial distance.

TABLE I
PROJECTED DIMENSIONS OF THE DESIGNED KA-BAND MALPFW-SWS

| Symbols | $a_0$ | $b_0$ | $r_0$ | $\theta$ |
|---|---|---|---|---|
| Values | 290 mm | 0.00045 | 268 mm | 2 deg |
| Symbols | $N$ | $a$ | $b$ | $r_c$ |
| Values | 81 | 5 mm | 0.45 mm | 0.34 mm |

In general, a proper positive tapering can improve the gain of the TWT. Therefore, the point of top gain should have a lower frequency than the PSP in the MALPFW-TWT. As a result, a conservative value of 2.5% is adopted as the spread limitation of the upper end considering the simulation results in Section III. This limitation is valuable while discussing the saturation output power and it can provide a preliminary guide for the design of the MALPFW-SWS.

If the input frequency falls out of frequency range of QSA, the TWT gain will decrease rapidly due to the fast variation of phase velocity. So, even the beam line crosses the "oscillation area" (such as the band edges shown in Fig. 2), the oscillation will be suppressed as the oscillation frequency is outside of the QSA range.

In addition, as mentioned in [2], the simplified dispersion equation (eq. (4)) deviated from the experiment measurements by about 1%-2% because the effects of circuit bends and beam holes were not taken into account. If needed, the more accurate dispersion curves can be obtained by simulation methods. The difference between the simulation results and the analytic equations are also shown in Fig.2.

## III. Design and Simulation Results

In order to validate the theory proposed in Section II, a Ka-band MALPFW-SWS is designed and studied by using PIC simulation.

Table I shows the projected dimensions of the designed SWS. $N$ is the total unit number of the SWS. According to the analytic expressions presented in Section II, the normalized phase velocity of the PSP is 0.152, corresponding to an optimized operating beam voltage of 6.9 kV.

An ideal round electron emitter, with a radius of 0.27 mm, was built in the PIC simulation to provide a round electron beam with current of 300 mA. A solenoid magnetic field of 0.4 T is applied to focus the electron beam.

The output power is calculated as 217 W when the input power is 18 mW at the frequency point of 32.4 GHz, as shown in Fig. 4. The output signal is very steady in the simulation

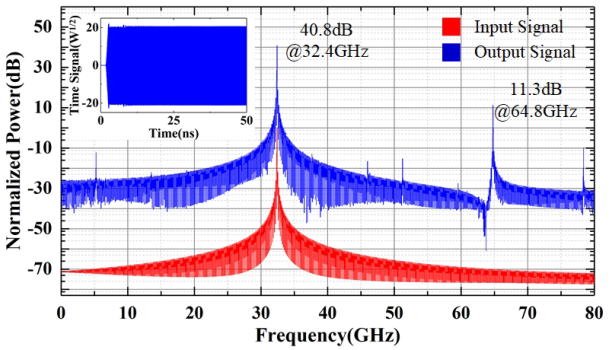


Fig. 4. Frequency spectrums of the input and output signals.

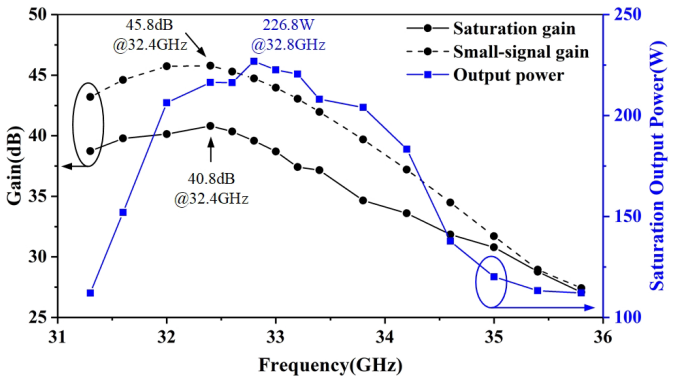


Fig. 5. Saturation output power, saturation gain and small-signal gain versus frequency.

duration time of 50 ns, even the gain of the one-section MALPFW-TWT has reached 40.8 dB. The corresponding frequency spectrums shown in Fig. 4 also proved that there is no obvious oscillation.

Fig. 5 shows the variations of the saturation input/output power, saturation/small-signal gain with frequency.

One can find out that the 3-dB frequency band of the saturation output power is 31.3-35.8 GHz from the blue line shown in Fig. 5. Furthermore, the small-signal gain obtained by fixing input power to 50 $\mu$W and sweeping frequency indicates that the 3-dB frequency band of small-signal gain is 31.3-33.2 GHz. The maximal small-signal gain is 45.8 dB, showing up at 32.4 GHz and this frequency is lower than the predicted PSF.

## IV. Cold Test Experiment

The fabrication of the Ka-band MALPFW-SWS is realized by dividing the SWS into two identical substructures from the middle plane of the broader side of waveguide. The fabricated components, including the mentioned substructures, a pair of flanges, a pair of connectors, a pair of transition waveguides and a copper sleeve, are shown in Fig. 6 (a).

Fig. 7 is the comparison between the simulation and experiment results of the S-parameters. The experiment results show that the $S_{11}$ is better than -15 dB and the $S_{21}$ is about -3.5 dB between the frequency range of 32.5-40 GHz. Fig. 8 provides the phase and loss curves. The average loss in axial direction is about 0.41 dB/cm – 0.58 dB/cm. The experiment results showed a good agreement in tendency with simulation results. It indicates that the fabricated Ka-Band MALPFW-SWS is of good transmission and is ready for hot test.

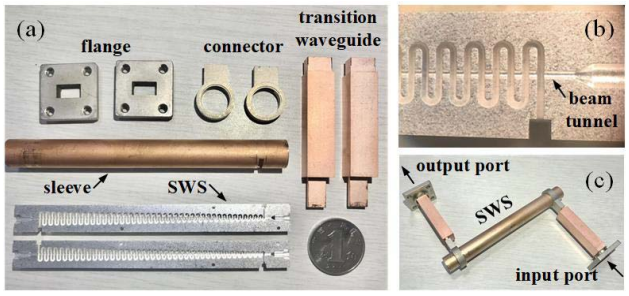


Fig. 6. Photos of (a) the fabricated components, (b) the profile of the MALPFW-SWS and (c) the fabricated MALPFW slow wave system.

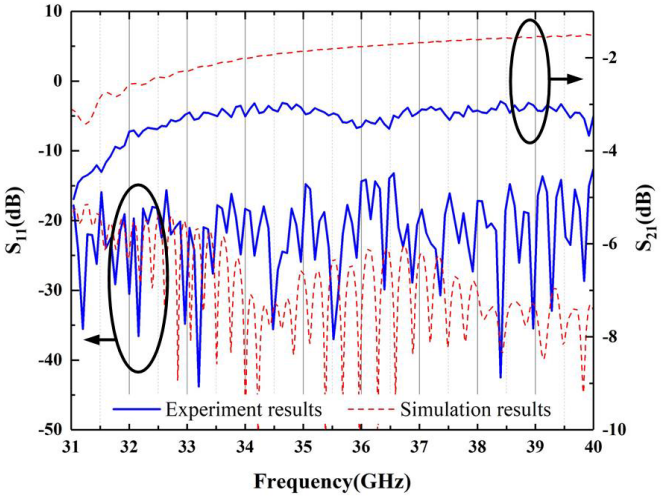


Fig. 7. Experiment results and simulation results of transmission characteristics.

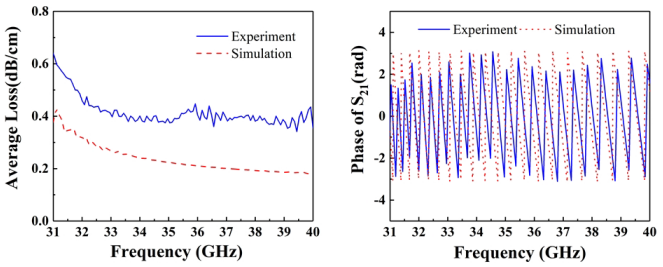


Fig. 8. (a) Insertion losses and (b) the phases of $S_{21}$.

## V. Conclusion

A novel SWS called MALPFW-SWS has been proposed in this letter. The theory analysis of the dispersion characteristics and cold test result have been presented for the MALPFW-SWS. The designed one-section MALPFW-SWS can achieve a high gain up to 40.8 dB from simulation, without obvious oscillation. The peak output power is 226.8 W at the frequency of 32.8 GHz. That indicated that the MALPFW-SWS can reduce the fabrication difficulty of the FW-TWT. The 3-dB frequency band of the saturation output power is 31.3-35.8 GHz.

The proposed MALPFW-SWS is more suitable for W band or THz band TWT. As no attenuator or cutoff is required, the structure of the proposed MALPFW-SWS is much simpler. Thus, the fabrication process can be simplified and the cost can be reduced significantly.

## REFERENCES


[1] S. Bhattacharjee, J. H. Booske, C. L. Kory, D. W. van der Weide, S. Limbach, S. Gallagher, J. D. Welter, M. R. Lopez, R. M. Gilgenbach, R. L. Ives, M. E. Read, R. Divan, and D. C. Mancini, "Folded waveguide traveling-wave tube sources for terahertz radiation," *IEEE Trans. Plasma Sci.*, vol. 32, no. 3, pp. 1002–1014, Jun. 2004, doi: 10.1109/TPS.2004.828886.

[2] J. H. Booske, M. C. Converse, C. L. Kory, C. T. Chevalier, D. A. Gallagher, K. E. Kreischer, V. O. Heinen, and S. Bhattacharjee, "Accurate parametric modeling of folded waveguide circuits for millimeter-wave traveling wave tubes," *IEEE Trans. Electron Devices*, vol. 52, no. 5, pp. 685–694, May 2005, doi: 10.1109/TED.2005.845798.

[3] R. K. Sharma, A. Grede, S. Chaudhary, V. Srivastava, and H. Henke, "Design of folded waveguide slow-wave structure for *W*-band TWT," *IEEE Trans. Plasma Sci.*, vol. 42, no. 10, pp. 3430–3436, Oct. 2014, doi: 10.1109/TPS.2014.2352267.

[4] K. T. Nguyen, A. N. Vlasov, L. Ludeking, C. D. Joye, A. M. Cook, J. P. Calame, J. A. Pasour, D. E. Pershing, E. L. Wright, S. J. Cooke, B. Levush, D. K. Abe, D. P. Chernin, and I. A. Chernyavskiy, "Design methodology and experimental verification of Serpentine/Folded-waveguide TWTs," *IEEE Trans. Electron Devices*, vol. 61, no. 6, pp. 1679–1686, Jun. 2014, doi: 10.1109/TED.2014.2303711.

[5] H. Gong, Y. Gong, T. Tang, J. Xu, and W.-X. Wang, "Experimental investigation of a high-power ka-band folded waveguide traveling-wave tube," *IEEE Trans. Electron Devices*, vol. 58, no. 7, pp. 2159–2163, Jul. 2011, doi: 10.1109/TED.2011.2148119.

[6] P. Hu, W. Lei, Y. Jiang, Y. Huang, R. Song, H. Chen, and Y. Dong, "Development of a 0.32-THz folded waveguide traveling wave tube," *IEEE Trans. Electron Devices*, vol. 65, no. 6, pp. 2164–2169, Jun. 2018, doi: 10.1109/TED.2017.2787682.

[7] J. Cai, J. Feng, Y. Hu, X. Wu, Y. Du, and J. Liu, "10 GHz bandwidth 100 watt W-Band folded waveguide pulsed TWTs," *IEEE Microw. Wireless Compon. Lett.*, vol. 24, no. 9, pp. 620–621, Sep. 2014, doi: 10.1109/LMWC.2014.2328891.

[8] W. Wang, *Microwave Engineering Technology*. Beijing, China: National Defense Industry Press, 2014, pp. 332–333.

[9] Z. Duan, Y. Gong, W. Wang, Y. Wei, and M. Huang, "Effect of attenuation on backward-wave oscillation start oscillation condition," *IEEE Trans. Plasma Sci.*, vol. 32, no. 6, pp. 2184–2188, Dec. 2004, doi: 10.1109/TPS.2004.838619.

[10] K. Guo, *Physical and Theoretical Problems on Traveling Wave Tubes*. Beijing, China: Publishing House of Electronic Industry, 2011, pp. 65–67.

[11] S. Wang, Y. Gong, Y. Hou, Z. Wang, Y. Wei, Z. Duan, and J. Cai, "Study of a log-periodic slow wave structure for ka-band radial sheet beam traveling wave tube," *IEEE Trans. Plasma Sci.*, vol. 41, no. 8, pp. 2277–2282, Aug. 2013, doi: 10.1109/TPS.2013.2271639.

[12] T. K. Ghosh, A. J. Challis, A. Jacob, and D. Bowler, "Design of helix pitch profile for broadband traveling-wave tubes," *IEEE Trans. Electron Devices*, vol. 56, no. 5, pp. 1135–1140, May 2009, doi: 10.1109/TED.2009.2015137.

[13] Z. Y. Duan, Y. B. Gong, Y. Y. Wei, W. X. Wang, B.-I. Wu, and J. A. Kong, "Efficiency improvement of broadband helix traveling wave tubes using hybrid phase velocity tapering model," *J. Electromagn. Waves Appl.*, vol. 22, no. 7, pp. 1013–1023, Jan. 2008, doi: 10.1163/156939308784150119.

[14] S.-S. Jung, A. V. Soukhov, B. Jia, G.-S. Park, and B. N. Basu, "Efficiency enhancement and harmonic reduction of wideband helix traveling-wave tubes with positive phase velocity tapering," *Jpn. J. Appl. Phys.*, vol. 41, no. Part 1, No. 6A, pp. 4007–4013, Jun. 2002, doi: 10.1143/JJAP.41.4007.

[15] T. K. Ghosh, A. J. Challis, A. Jacob, D. Bowler, and R. G. Carter, "Improvements in performance of broadband helix traveling-wave tubes," *IEEE Trans. Electron Devices*, vol. 55, no. 2, pp. 668–673, Feb. 2008, doi: 10.1109/TED.2007.913006.